

# Effects of nonquadrupole modes in the detection and parameter estimation of black hole binaries with nonprecessing spins

Vijay Varma\*

*Theoretical Astrophysics, California Institute of Technology, Pasadena, California 91125, USA*

Parameswaran Ajith

*International Centre for Theoretical Sciences, Tata Institute of Fundamental Research, Bangalore 560089, India and  
Canadian Institute for Advanced Research, CIFAR Azrieli Global Scholar, MaRS Centre,  
West Tower, 661 University Avenue, Suite 505, Toronto, Ontario M5G 1M1, Canada*

We study the effect of nonquadrupolar modes in the detection and parameter estimation of gravitational waves (GWs) from black hole binaries with nonprecessing spins, using Advanced LIGO. We evaluate the loss of the signal-to-noise ratio (SNR) and the systematic errors in the estimated parameters when a quadrupole-mode template family is used to detect GW signals with all the relevant modes. Target signals including nonquadrupole modes are constructed by matching numerical-relativity simulations of nonprecessing black hole binaries describing the late inspiral, merger and ringdown with post-Newtonian/effective-one-body waveforms describing the early inspiral. We find that neglecting nonquadrupole modes will, in general, cause unacceptable loss in the detection rate and unacceptably large systematic errors in the estimated parameters, for the case of massive binaries with large mass ratios. For a given mass ratio, neglecting subdominant modes will result in a larger loss in the detection rate for binaries with aligned spins. For binaries with antialigned spins, quadrupole-mode templates are more effectual in detection, at the cost of introducing a larger systematic bias in the parameter estimation. We provide a summary of the regions in the parameter space where neglecting nonquadrupole modes will cause an unacceptable loss of detection rates and unacceptably large systematic biases in the estimated parameters.

## I. INTRODUCTION AND SUMMARY

We are firmly in the era of gravitational wave (GW) astronomy, with LIGO having made two confident detections of binary black holes [1, 2] and many more expected in upcoming observing runs [3, 4]. Indeed, these first observations have already given us a glimpse of the unique capabilities of GW astronomy. Apart from providing the first direct evidence of the existence of GWs, these observations confirmed the existence of stellar mass black holes that are much more massive than commonly thought by astronomers [5, 6]. They also provided the first evidence of black hole binaries that inspiral under GW emission and merge within the age of the Universe. These observations also enabled us to perform the first tests of GR in the highly relativistic and nonlinear regime of gravity – a regime inaccessible by other astronomical observations and laboratory tests [7].

The first LIGO event, termed GW150914, was produced by the merger of two massive black holes. The resultant signal in the detectors contained imprints of the late inspiral and merger of the two holes and the subsequent ringdown of the remnant black hole. The signal was first detected by two low-latency searches for generic transient signals that are coherent in multiple detectors [8–11]. The signal was later confirmed with higher confidence by matched filter-based searches that use relativistic models of expected signals from coalescing compact binaries [12–15]. The second signal was produced by the coalescence of two less massive black holes, and the resultant signal in the detector predominantly consisted of the long inspiral. Hence matched filter-based searches were essential for its detection [2].

Matched-filtering is the most sensitive search method for extracting signals of known signal shape from noisy data, such as the GW signals from the coalescence (inspiral, merger and ringdown) of binary black holes. The source parameters are then extracted by comparing the data against theoretical tem-

plates by means of Bayesian inference [5, 16]. Our ability to optimally detect the signal using matched-filtering and to estimate the source parameters using Bayesian inference depends crucially on how faithfully the theoretical templates model the signal present in the data. If the template is a poor representation of the true signal, this can reduce the matched-filtering signal-to-noise ratio (SNR), potentially causing nondetection and/or causing unacceptable systematic biases in the estimated parameters. Good waveform templates should be not only *effective* in the detection (small loss in the SNR) but also *faithful* in parameter estimation (small systematic biases) [17].

Matched filter-based searches for GWs performed to date, including the ones that resulted in detections, have employed templates that model only the leading (quadrupole, or  $\ell = 2$ ,  $m = \pm 2$ ) spherical harmonic modes of the GWs radiated from the binary. The parameter estimation exercise also has largely employed quadrupole mode templates (with the notable exception of one that directly employed numerical-relativity (NR) waveforms [19]). This choice is partly dictated by the unavailability of fast-to-evaluate, semianalytical waveform templates describing the inspiral, merger and ringdown of binary black holes that model the subdominant (nonquadrupole) modes over a sufficiently wide region in the parameter space (e.g., spinning binaries). More importantly, several studies in the past have suggested that the contribution from subdominant modes are appreciable only for very massive binaries with large mass ratios [18, 20–22]. The effect of subdominant modes was thoroughly investigated in the context of GW150914, and the study concluded that the effect of subdominant modes is negligible in the detection and parameter estimation of this event [23, 24].

In a previous study [18], we investigated the effect of subdominant modes in the detection and parameter estimation of a population of nonspinning black hole binaries. Here, we extend our previous study to the case of black hole binaries with nonprecessing spins<sup>1</sup>. We construct target GW signals that

<sup>1</sup>We note that, in a recent paper, Calderon-Bustillo *et al* [25] extended our previous study of nonspinning binaries to the case of spinning binaries with

\*Electronic address: [vvarma@caltech.edu](mailto:vvarma@caltech.edu)

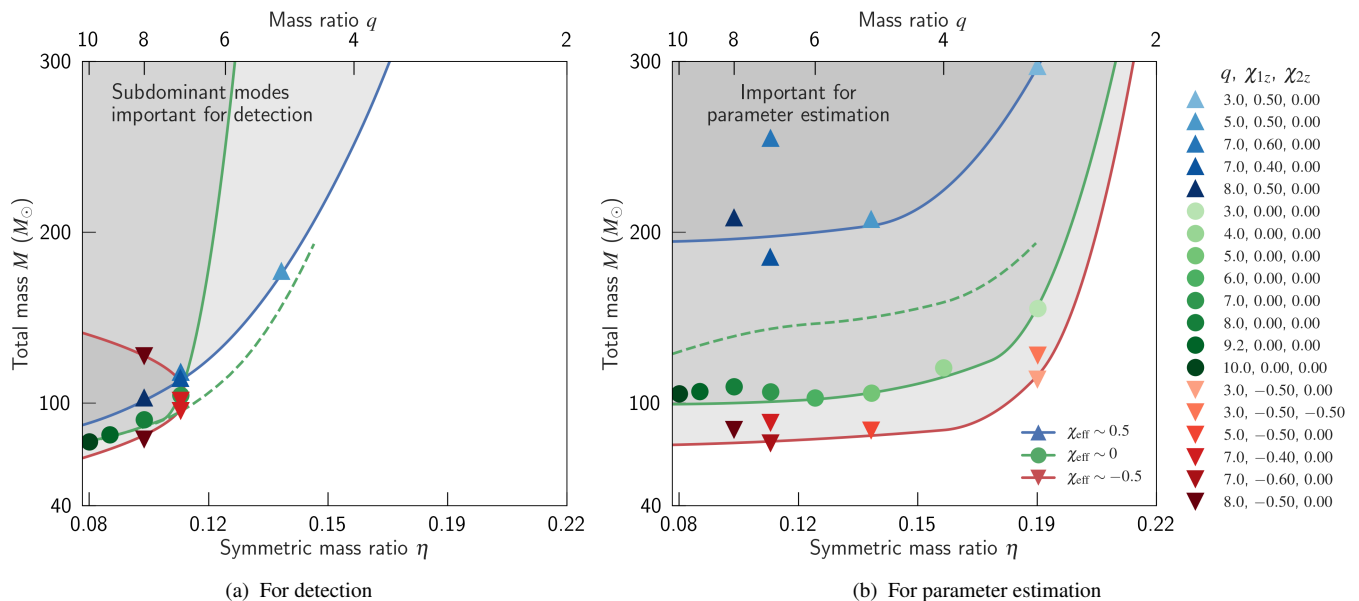


FIG. 1: These plots summarize the region in the parameter space of nonprecessing black-hole binaries where contributions from subdominant modes are important for detection (left) and parameter estimation (right). In the left panel, the shaded areas show the regions in the parameter space where the loss of detection volume (for a fixed SNR threshold) due to neglecting subdominant modes is larger than 10%. In the right panel, shaded areas show the regions in the parameter space where the systematic errors in any of the estimated parameters [total mass  $M := m_1 + m_2$ , symmetric mass ratio  $\eta := m_1 m_2 / M^2$  and effective spin parameter  $\chi_{\text{eff}} := (m_1 \chi_1 + m_2 \chi_2 / M)$ ] are larger than the expected statistical errors for a sky and orientation-averaged SNR of 8 (corresponding to an optimal orientation SNR  $\approx 20$ ). In each plot the three solid curves correspond to different effective spin values: blue for  $\chi_{\text{eff}} \sim 0.5$ , green for  $\chi_{\text{eff}} \sim 0$  and red for  $\chi_{\text{eff}} \sim -0.5$ . The left panel was made by computing the fitting factors of dominant-mode templates including nonprecessing spins with hybrid waveforms including all the relevant modes, and the right panel was made making use of averaged systematic biases. The markers (triangles pointing up/down denoting binaries with aligned/antialigned spins and circles denoting nonspinning binaries) indicate the data points that are used to construct the shaded regions and curves. The legend shows the mass ratios and spins of the target signals featured in these plots. See Sec. I for a summary and Sec. III for a detailed discussion. For comparison, the dashed green lines show the same results for nonspinning binaries using a nonspinning template family from our previous work [18].

include subdominant modes ( $\ell \leq 4, m \neq 0$ ) by matching nonprecessing numerical-relativity simulations describing the late inspiral, merger and ringdown with post-Newtonian/effective-one-body waveforms describing the early inspiral. We then compute the reduction in the detectable volume (for a fixed SNR threshold) and systematic bias in the estimated parameters when nonprecessing quadrupole-mode only templates are employed in the detection and parameter estimation of these target waveforms.

Figure 1 summarizes the main results from this study. The left plot shows the region in the parameter space where neglecting subdominant modes will cause an unacceptable (more than 10%) loss in the detectable volume (appropriately averaged over all orientation and sky location angles) for a fixed SNR threshold. The right plot shows the region in the parameter space where neglecting subdominant modes will cause unacceptably large systematic bias in the parameter estimation (i.e., systematic errors larger than the expected statistical errors for a sky and orientation-averaged SNR of 8). Comparing these results with our previous study employing nonspinning tem-

plates (i.e., by comparing the dashed green curve with the solid green curve in the left plot of Fig. 1), we see that including spin effects in the dominant-mode templates enhances their effectualness, thus reducing the region in the parameter space where subdominant mode templates are required for detection. However, this is achieved at the cost of introducing larger systematic errors in the estimated parameters, thus increasing the volume of the parameter space where subdominant mode templates should be used in the parameter estimation. This effect (better effectualness at the cost of larger systematic errors) is more pronounced in the case of binaries with spins *antialigned* with the orbital angular momentum. Thus, subdominant-mode templates are required for detection of binaries with antialigned spins only over a small region in the parameter space; but they are required for parameter estimation over a large region. This effect is reversed in the case of *aligned* spins.

The rest of this paper is organized as follows: Section II provides details of the methodology and figures of merit for this study. Section III discusses our results including how we arrive at Fig. 1. Finally, Sec. IV has some concluding remarks, limitations of this work and targets for future work. Appendix A presents a comparison of our estimates of the statistical and systematic errors with the same estimated from fully Bayesian parameter estimation for one sample case. Please note our notation for the rest of this article:  $M$  refers to the total mass of the binary,  $m_1$  and  $m_2$  ( $m_1 \geq m_2$ ) refer to the component masses, and  $\chi_1$  and  $\chi_2$  refer to the dimensionless spin parameters;

equal component spins. Our new study covers a larger region in the parameter space, by employing numerical-relativity waveforms with larger mass ratios and spins. The template family that we use also can span a large spin range ( $\chi_{1z,2z} \in [-1, 1]$  as opposed to  $\chi \in [-1, 0.6]$  employed in [25]); hence we see better fitting factors at the cost of a larger parameter bias.

Simulation ID	$q$	$\chi_{1z}$	$\chi_{2z}$	$M\omega_{\text{orb}}$	Number of orbits
SXS:BBH:0172	1	0.98	0.98	0.015	25.4
SXS:BBH:0160	1	0.90	0.90	0.015	24.8
SXS:BBH:0155	1	0.80	0.80	0.015	24.1
SXS:BBH:0152	1	0.60	0.60	0.016	22.6
SXS:BBH:0090	1	0.00	0.00	0.011	32.4
SXS:BBH:0151	1	-0.60	-0.60	0.016	14.5
SXS:BBH:0154	1	-0.80	-0.80	0.016	13.2
SXS:BBH:0159	1	-0.90	-0.90	0.016	12.7
SXS:BBH:0156	1	-0.95	-0.95	0.016	12.4
SXS:BBH:0253	2	0.50	0.50	0.014	28.8
SXS:BBH:0047	3	0.50	0.50	0.017	22.7
SXS:BBH:0174	3	0.50	0.00	0.013	35.5
SXS:BBH:0110	5	0.50	0.00	0.019	24.2
SXS:BBH:0202	7	0.60	0.00	0.013	62.1
SXS:BBH:0203	7	0.40	0.00	0.013	58.5
SXS:BBH:0065	8	0.50	0.00	0.019	34.0
SXS:BBH:0184	2	0.00	0.00	0.018	15.6
SXS:BBH:0183	3	0.00	0.00	0.020	15.6
SXS:BBH:0167	4	0.00	0.00	0.021	15.6
SXS:BBH:0056	5	0.00	0.00	0.016	28.8
SXS:BBH:0181	6	0.00	0.00	0.018	26.5
SXS:BBH:0298	7	0.00	0.00	0.021	19.7
SXS:BBH:0063	8	0.00	0.00	0.019	25.8
SXS:BBH:0189	9.2	0.00	0.00	0.021	25.2
SXS:BBH:0185	10	0.00	0.00	0.021	24.9
SXS:BBH:0238	2	-0.50	-0.50	0.011	32.0
SXS:BBH:0036	3	-0.50	0.00	0.012	31.7
SXS:BBH:0046	3	-0.50	-0.50	0.018	14.4
SXS:BBH:0109	5	-0.50	0.00	0.020	14.7
SXS:BBH:0205	7	-0.40	0.00	0.013	44.9
SXS:BBH:0207	7	-0.60	0.00	0.014	36.1
SXS:BBH:0064	8	-0.50	0.00	0.020	19.2

TABLE I: Summary of the parameters of the NR waveforms used in this paper:  $q \equiv m_1/m_2$  is the mass ratio of the binary,  $\chi_{1z}$  and  $\chi_{2z}$  are the dimensionless spins of the larger and smaller black holes respectively, and  $M\omega_{\text{orb}}$  is the orbital frequency after the junk radiation. All of these waveforms have residual eccentricity,  $e < 4 \times 10^{-3}$  (typically significantly smaller).

$\chi_{1,2} = S_{1,2}/m_{1,2}^2$  where  $S_{1,2}$  are the spin angular momenta of the components. All masses are detector frame (redshifted) masses. We only consider spins aligned/antialigned with the orbital angular momentum. The mass ratio is denoted by  $q = m_1/m_2$  while  $\eta = m_1 m_2 / M^2$  denotes the symmetric mass ratio. We also define the effective spin parameters  $\chi_{\text{eff}} = (m_1 \chi_1 + m_2 \chi_2) / M$  and  $\tilde{\chi}_{\text{eff}} = (m_1 \chi_1 - m_2 \chi_2) / M$ . We refer to waveforms that include contributions from sub-dominant modes ( $\ell \leq 4, m \neq 0$ ) as “full” waveforms and waveforms that include only quadrupole modes ( $\ell = 2, m = \pm 2$ ) as “quadrupole” waveforms. We refer to the SNR averaged over orientation and inclination angles as the orientation-averaged SNR; note that SNR along optimal orientation is  $\sim 2.5$  times the orientation-averaged SNR [26].

## II. METHODOLOGY

In a past study [18], we investigated the effects of non-quadrupole modes in the detection and parameter estimation of nonspinning binaries. Here we extend the earlier work to the case of nonprecessing binaries, covering a wide range of total masses ( $40M_{\odot} \leq M \leq 300M_{\odot}$ ), mass ratios ( $q \leq 10$ ) and spins ( $-0.5 \leq \chi_{\text{eff}} \leq 0.5$  for  $q \geq 2$  and  $-0.95 \leq \chi_{\text{eff}} \leq 0.98$  for  $q = 1$ ). For our target signals, we use hybrid waveforms constructed by

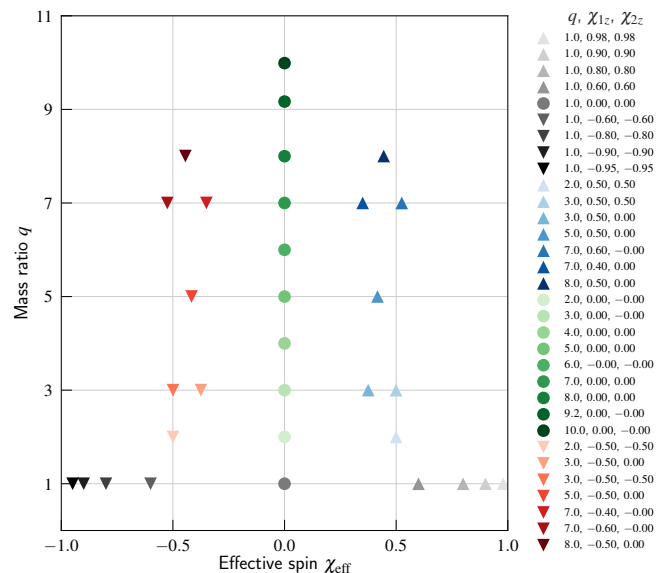


FIG. 2: This plot shows the mass ratio (vertical axis) and effective spin (horizontal axis) of the NR waveforms used in this study. The color scheme of the markers is same as that in Figs. 1, 6 and 8, enabling direct comparison.

matching NR waveforms that describe the late inspiral, merger and ringdown of binary black holes with post-Newtonian (PN) / effective-one-body (EOB) waveforms modeling the early inspiral. These hybrids contain several nonquadrupolar modes ( $\hat{h}_{\ell m}(t)$  with  $\ell \leq 4, |m| \leq \ell, m \neq 0$ ) of GW signals from binary black holes. The PN waveforms were generated using the 3PN amplitude given by [27–29], but using the phase evolution given by the SEOBNRv2 waveform family<sup>2</sup> [30]. We match them with NR waveforms produced by the SpEC [31–47] code by the SXS Collaboration that are available at the public SXS catalog of NR waveforms [31]. The parameters of the NR waveforms used in this study are shown in Table I and Fig. 2. Note that the  $(\ell, m) = (4, 1)$  mode in several of the NR waveforms has significant numerical noise. However, as the amplitude of this mode is several orders of magnitude smaller than that of the dominant mode, we do not expect this to impact our results.

As described in detail in our past study [18], to construct hybrids, we match the PN modes  $\hat{h}_{\ell m}^{\text{PN}}(t)$  with NR modes  $\hat{h}_{\ell m}^{\text{NR}}(t)$  by a least square fit over two rotations ( $\varphi_0, \psi$ ) on the NR mode and the time difference between NR and PN modes:

$$\Delta = \min_{t_0, \varphi_0, \psi} \int_{t_1}^{t_2} dt \sum_{\ell, m} \left| \hat{h}_{\ell m}^{\text{NR}}(t - t_0) e^{i(m\varphi_0 + \psi)} - \hat{h}_{\ell m}^{\text{PN}}(t) \right|. \quad (2.1)$$

The hybrid modes are constructed by combining the NR modes with the “best-matched” PN modes:

$$\hat{h}_{\ell m}^{\text{hyb}}(t) \equiv \tau(t) \hat{h}_{\ell m}^{\text{NR}}(t - t'_0) e^{i(m\varphi'_0 + \psi')} + (1 - \tau(t)) \hat{h}_{\ell m}^{\text{PN}}(t), \quad (2.2)$$

where  $t'_0, \varphi'_0$  and  $\psi'$  are the values of  $t_0, \varphi_0$  and  $\psi$  that minimizes the difference  $\Delta$  between PN and NR modes and  $\tau(t)$  is a suitable weighting function that smoothly goes from 0 to 1

<sup>2</sup>This was done in order to make the phase evolution of the hybrids very similar to that of the templates, so that a mismatch between the hybrid and the template due to the different phase evolution will not be mistaken as due to the effect of subdominant modes.



during the interval  $t_1 \leq t \leq t_2$ . We refer the reader to Ref. [18] for details about the construction of hybrid waveforms. An example of hybrid waveform modes is shown in Fig. 3. It can be seen that higher modes are excited only during the very late inspiral, merger and ringdown. The effect of higher modes will be appreciable only in the mass range where the SNR contributed by the merger-ringdown is a significant fraction of the total SNR. This is the reason we restrict our study to the mass range  $40M_\odot \leq M \leq 300M_\odot$ ; we do not see any evidence of a significant impact of higher modes for binaries with lower masses. Since the NR waveforms we use include tens of cycles in the inspiral, we do not expect hybridization errors to impact our results, particularly for high masses. For a detailed study on hybridization errors, we refer the reader to Refs. [48–52].

The template family used is IMRPhenomD [53, 54], which is a quadrupole-only ( $\ell = 2, m = \pm 2$ ) inspiral, merger and ringdown waveform family described by two mass parameters and two nonprecessing spin parameters. These waveforms are calibrated to NR waveforms with  $q \leq 18$ ,  $|\chi_{1z,2z}| \lesssim 0.85$  (0.98 for  $q = 1$ ) and we find that they have a very good agreement with the quadrupole modes of the hybrid waveforms discussed above (cf. the dashed lines in Fig. 6). The waveforms are generated in the Fourier-domain using the LALSimulation [55] software package.

We compute fitting factors [56] by maximizing the overlap (noise weighted inner product) of the template family against the target hybrid signals and infer the systematic errors by comparing the best-match parameters with the true parameters. The overlaps are maximized over the extrinsic parameters (time of arrival  $t_0$  and the reference phase  $\varphi_0$ ) using the standard techniques in GW data analysis (see, e.g., Ref. [57]), while the overlaps are maximized over the intrinsic parameters ( $M, \eta, \chi_{1z}$  and  $\chi_{2z}$ ) of the templates using a Nelder-Mead downhill simplex algorithm [58], with additional enhancements described in Ref. [18]. For the model of the noise power spectrum, we use the “zero-detuned, high-power” design noise power spectral density (PSD) [59] of Advanced LIGO with a low frequency cut-off of 20 Hz.

The contribution of subdominant modes in the observed signal depends on the relative orientation of the binary and the detector. The SNR (and hence the volume in the local Universe where the binary can be confidently detected) is also a strong function of this relative orientation. For, e.g., binaries that are face-on produce the largest SNR in the detector; however, the contribution from subdominant modes is minimal for this orientation. This effect is reversed for the case of edge-on orientations. Thus, if we want to calculate the effect of subdominant modes on detection and parameter estimation of a population of binary black holes, the effect has to be averaged over all orientations after appropriately weighting each orientation.

We evaluate the *effective volume* [18] of a search, defined as the fraction of the volume that is accessible by an optimal search (corresponding to a fixed SNR threshold), by averaging over all the relative orientations in the following way:

$$V_{\text{eff}}(m_1, m_2, \chi_{1z}, \chi_{2z}) = \frac{\overline{\rho_{\text{opt}}^3 \text{FF}^3}}{\overline{\rho_{\text{opt}}^3}}, \quad (2.3)$$

where  $\rho_{\text{opt}}$  is the optimal SNR of the full signal, FF is the fitting factor of the dominant mode template, and the bars indicate averages over all (isotropically distributed) orientations<sup>3</sup>. The

dominant-mode template family is deemed effectual for detection when the effective volume is greater than 90%; or when the *effective fitting factor*  $\text{FF}_{\text{eff}} := V_{\text{eff}}^{1/3}$  is greater than 0.965.

Similarly, we define the *effective bias* [18] in estimating an intrinsic parameter  $\lambda$  as

$$\Delta\lambda_{\text{eff}}(m_1, m_2, \chi_{1z}, \chi_{2z}) = \frac{\overline{|\Delta\lambda| \rho_{\text{opt}}^3 \text{FF}^3}}{\overline{\rho_{\text{opt}}^3 \text{FF}^3}}, \quad (2.4)$$

where  $\Delta\lambda$  is the systematic bias in estimating the parameter  $\lambda$  for one orientation, FF is the corresponding fitting factor, and  $\rho_{\text{opt}}$  the corresponding optimal SNR. Here, also, the bars indicate averages over all orientations. The effective bias provides an estimate of the bias averaged over a population of detectable binaries with isotropic orientations. We compare them against the sky and orientation averaged statistical errors. Statistical errors are computed using the Fisher matrix formalism employing quadrupole-only templates. The quadrupole-mode template family is deemed faithful for parameter estimation when the effective biases in all of the three intrinsic parameters  $M, \eta, \chi_{\text{eff}}$  are smaller than the  $1\sigma$  statistical errors in measuring the same parameter for an orientation-averaged SNR of 8.

### III. RESULTS AND DISCUSSION

In this section, we evaluate the performance of the quadrupole-mode inspiral-merger-ringdown template family IMRPhenomD, against the “full” hybrid waveforms by computing the fitting factor of the template and inferring the parameter biases from the best-matched parameters. Figure 4 shows the optimal SNR of the hybrid waveforms and fitting factor of the quadrupole-mode templates at different values of  $\iota$  and  $\varphi_0$  (averaged over the polarization angle  $\psi$ ). Figure 5 shows the systematic bias in estimating parameters total mass  $M$ , symmetric mass ratio  $\eta$ , and effective spin  $\chi_{\text{eff}}$ , using the quadrupole-mode template family. It is clear that for the  $q = 1$  case (left column) the fitting factor is close to 1, and the systematic errors are negligible for all orientations, indicating the weak contribution of subdominant modes. For mass ratio 8, the fitting factor can be as low as  $\sim 0.84$  for binaries that are highly inclined ( $\iota \simeq \pi/2$ ) with the detector, where the contribution from nonquadrupole modes is the highest. However, these are the orientations where the SNR is the minimum (see Fig. 4). Similarly, the systematic biases are typically the largest (smallest) for the edge-on (face-on) configurations where the SNR is the smallest (largest). Hence GW observations are intrinsically biased toward orientations where the effect of nonquadrupole modes is minimum. This effect, in general, reduces the importance of nonquadrupole modes for a population of binaries that are oriented isotropically [18, 20–22]<sup>4</sup>.

Figure 6 shows the *ineffectualness* ( $1 - \text{FF}_{\text{eff}}$ ) and effective biases in estimated parameters as a function of the total mass

polarization angle  $\psi \in [0, 2\pi)$ , and the cosine of the inclination angle  $\cos \iota \in [-1, 1]$ . Note that we assume that the binaries are optimally located (i.e., the angles  $\theta, \phi$  describing the location of the binary in the detector frame on the sky are set to zero). The error introduced by this restriction is very small ( $\sim 0.1\%$ ) due to the weak dependence of the matches on  $(\theta, \phi)$  and the strong selection bias towards binaries with  $\theta \simeq 0, \pi$ , where the antenna pattern function peaks [18].

<sup>4</sup>Note that this is an artifact of the limited horizon distance of the second-generation GW detectors. For the case of third generation GW detectors, binaries with practically all orientations will be detected, thus eliminating this selection bias; see, e.g., [60]

<sup>3</sup>This corresponds to uniform distributions in the phase angle  $\varphi_0 \in [0, 2\pi)$ ,

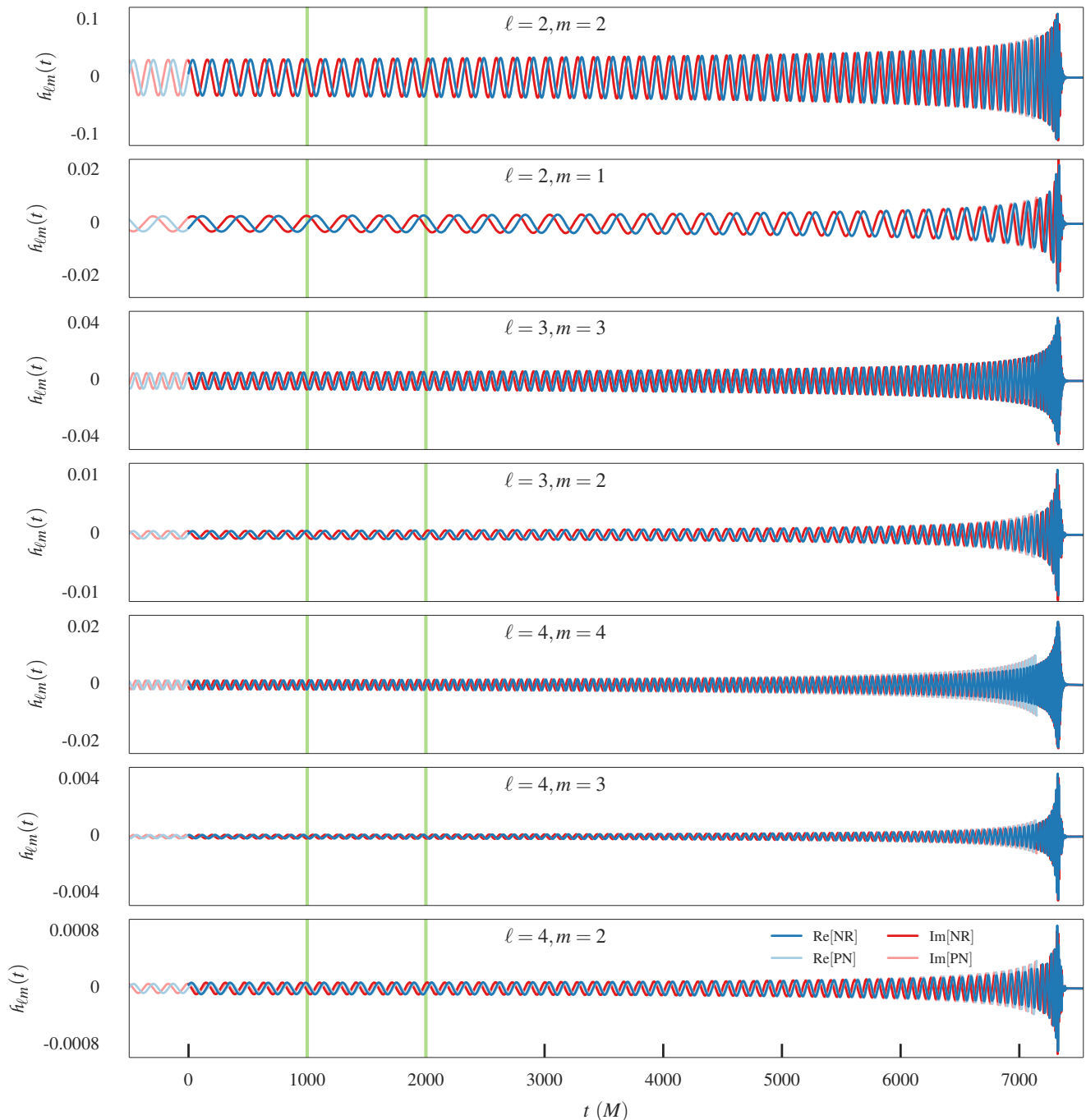


FIG. 3: Example of hybrid waveform modes constructed by matching NR and PN modes. These hybrid waveforms are constructed by matching  $q = 8$ ,  $\chi_{1z} = 0.5$ ,  $\chi_{2z} = 0$  NR waveforms computed using the SpEC code with PN/EOB waveforms describing the early inspiral. The horizontal axes show the time (with origin at the start of the NR waveforms) and the vertical axes show the GW modes  $h_{lm}(t)$ . The matching region ( $1000M, 2000M$ ) is marked by vertical green lines.

of the binary for different mass ratios and spins. For total mass  $M$  and symmetric mass ratio  $\eta$ , fractional biases are shown while for  $\chi_{\text{eff}}$  absolute biases are shown<sup>5</sup>. Solid (dashed) lines correspond to the case where “full” (quadrupole-only) hybrid waveforms are used as target waveforms. The template family

<sup>5</sup>In the case of anti-symmetric spin parameter  $\tilde{\chi}_{\text{eff}}$ , the biases are dominated by the bias in the quadrupole mode itself. This is expected as previous studies have shown that LIGO can only estimate  $\chi_{\text{eff}}$  to a good accuracy. Therefore we do not consider biases in  $\tilde{\chi}_{\text{eff}}$  in this study.

in both cases contains only the quadrupole mode. The difference between the solid and dashed lines indicates the effect of ignoring sub-dominant modes for detection and parameter estimation. Note that many of the dashed lines lie below the scale of these plots and are not displayed.

Previous studies [18, 20–22, 25] have shown that the effects of subdominant modes become important for binaries with high masses and large mass ratios. At large mass ratios, subdominant modes are excited by a larger extent due to higher asymmetry. For high masses, the observed signal is dominated by the merger, during which sub-dominant modes are excited prominently. Consistent with our expectation, in Fig. 6, the

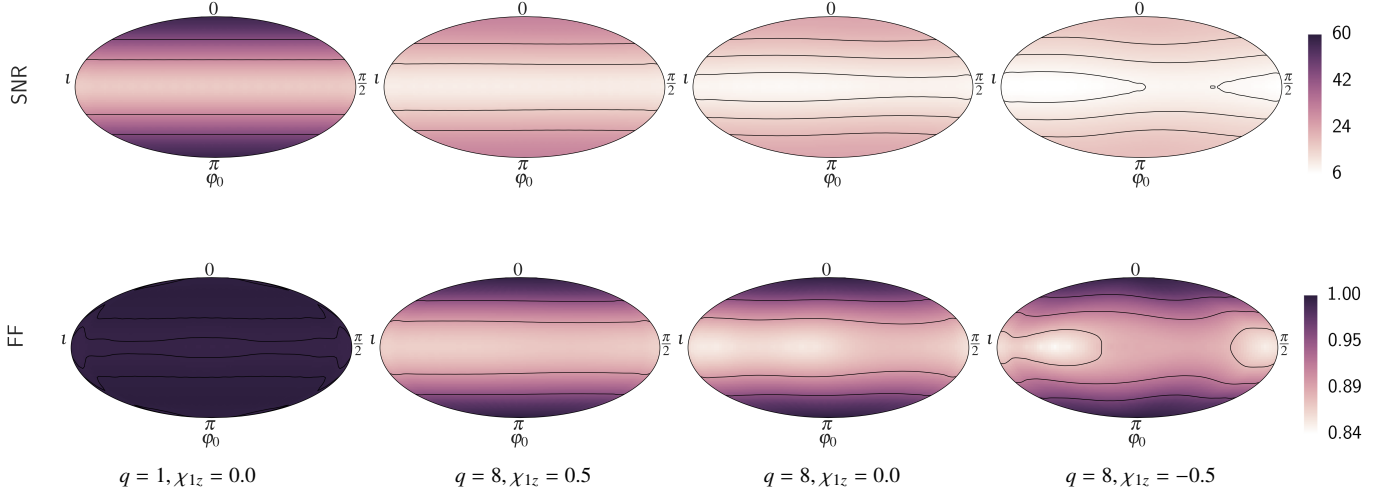


FIG. 4: Optimal SNR (top panel) and fitting factor of quadrupole templates (bottom panel), averaged over polarization angle  $\psi$  for binaries with total mass  $M = 100 M_{\odot}$ , located at 1 Gpc. The y-axis shows the inclination angle  $i$  in radians and the x-axis shows the initial phase of the binary  $\varphi_0$  in radians. The equator ( $i = \pi/2$ ) corresponds to “edge-on” orientation while the poles ( $i = 0, \pi$ ) correspond to “face-on” orientation. Different columns correspond to different mass ratios and spins of the larger black hole (the spin on the smaller black hole is 0 in all three cases). It may be noted that the fitting factor as well as the intrinsic luminosity are smallest (largest) at  $i = \pi/2$  ( $i = 0, \pi$ ) where contribution from the nonquadrupole modes is the largest (smallest), illustrating the selection bias toward configurations where nonquadrupole modes are less important.

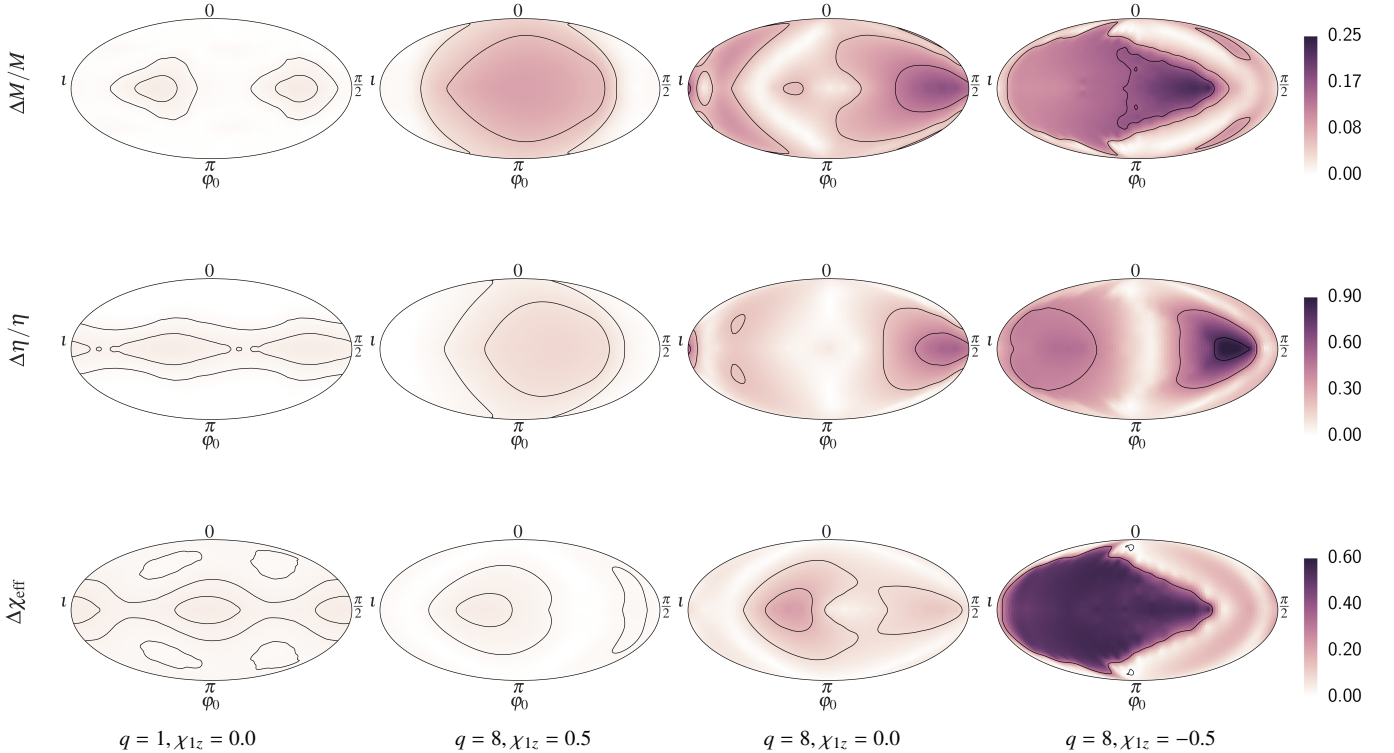


FIG. 5: Systematic bias in the estimation of total mass  $M$  (top panel), symmetric mass ratio  $\eta$  (middle panel), and effective spin  $\chi_{\text{eff}}$  (bottom panel), averaged over polarization angle  $\psi$  for binaries with total mass  $M = 100 M_{\odot}$ . For  $M$  and  $\eta$ , relative biases are shown, while for  $\chi_{\text{eff}}$  absolute biases are shown. The y-axis shows the inclination angle  $i$  in radians and the x-axis shows the initial phase of the binary  $\varphi_0$  in radians. Different columns correspond to different mass ratios and spins of the larger black hole (the spin on the smaller black hole is 0 in all three cases).

solid lines show that, in general, the ineffectualness and effective biases increase with increasing mass ratio and with increasing mass. We also see a clear separation of the solid and dashed lines for large mass ratios and high masses, illustrating

the effect of neglecting nonquadrupole modes.

Figure 6 also reveals an interesting dependence of the effect of nonquadrupole modes on the spins. For binaries with aligned, zero, and antialigned spins, the ineffectualness peaks

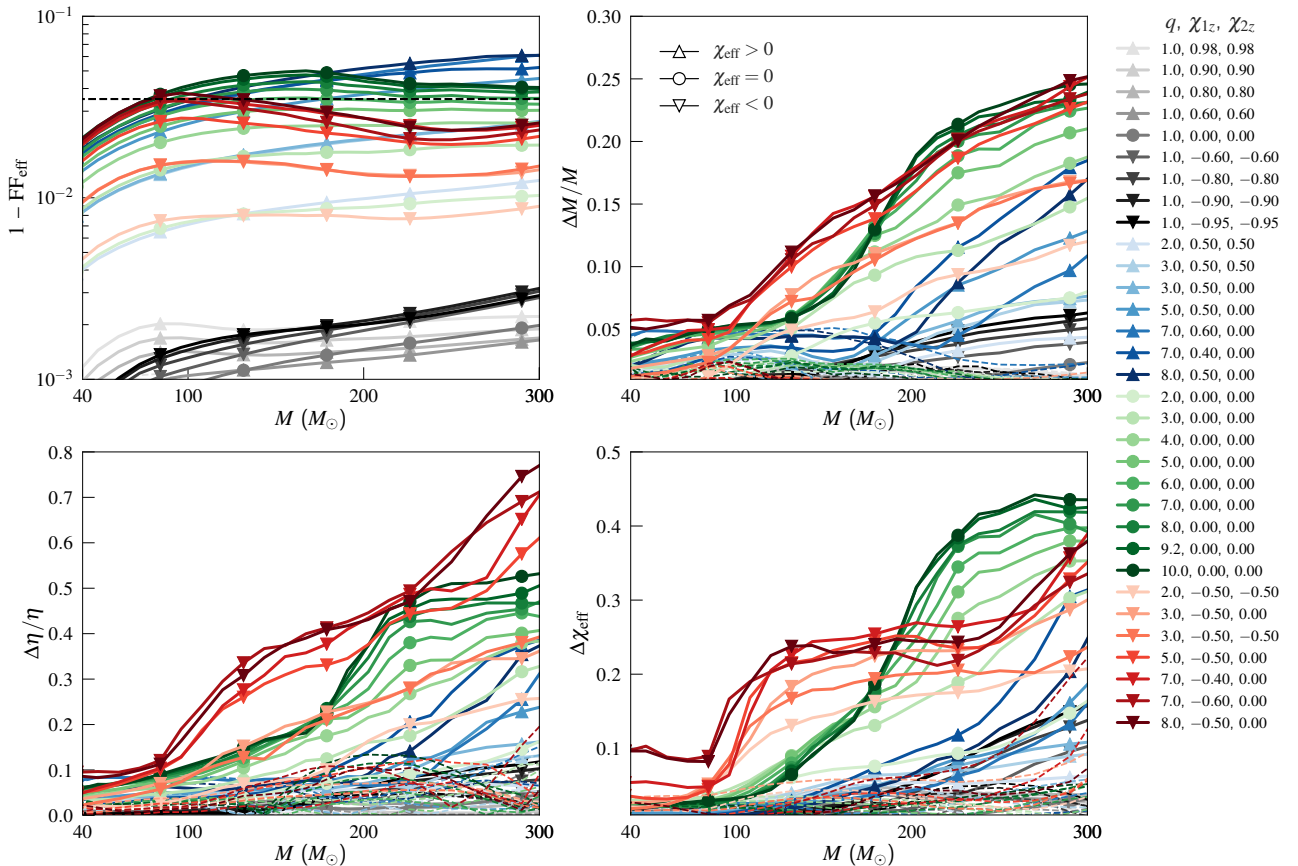


FIG. 6: “Ineffectualness” ( $1 - \text{FF}_{\text{eff}}$ ) and effective parameter biases when using quadrupole-mode templates against hybrid waveforms including all modes. Dashed lines correspond to the same but against quadrupole-only hybrid waveforms, so that the difference between the dashed and solid lines gives an indication of the effect of nonquadrupole modes. Fractional biases are shown for total mass  $M$  and symmetric mass ratio  $\eta$ , while absolute biases are shown for effective spins  $\chi_{\text{eff}}$ .  $\text{FF}_{\text{eff}}$  and effective parameter biases are obtained by averaging over all relevant orientations of the binary using Eqs. (2.3) and (2.4). The horizontal axis reports the total mass of the binary while the mass ratio and spins are shown in the legend. The markers indicate the spin types: triangles pointing up/down denoting binaries with aligned/antialigned spins and circles denoting nonspinning binaries. The horizontal dashed black line corresponds to  $1 - \text{FF}_{\text{eff}}^3 = 0.1$ . Note that most of the dashed lines in the top-left subplot lie below  $10^{-3}$ . We see that as the total mass increases, the ineffectualness and effective biases in  $M$ ,  $\eta$  and  $\chi_{\text{eff}}$  increase and are dominated by the effects of subdominant modes; see Sec. III for further discussion.

at total masses of  $M \sim 300M_{\odot}$ ,  $M \sim 150M_{\odot}$ ,  $M \sim 100M_{\odot}$ , respectively<sup>6</sup>. This is roughly the mass range where the observed signal is dominated by the late inspiral and merger – the phase where the higher modes are excited most prominently. For binaries with antialigned spins, merger happens at relatively lower frequencies, while, for the case of aligned spins, merger happens at relatively higher frequencies, owing to the “orbital hangup” [61, 62] effect. Since frequencies are scaled inversely to the total mass of the system, this creates the mass dependence of the ineffectualness that we describe above. For very high masses, the observed signal will contain only the ring-down phase. Due to the smaller bandwidth and the relatively simpler structure of the ringdown signal, the quadrupole-only templates are likely to be able to mimic the full ringdown signal relatively well, at the cost of considerable systematic errors (see Fig. 7 for an example). Hence, we anticipate the effectualness of the quadrupole-mode templates to go up at very high masses. This effect should start dominating the effectualness patterns at relatively lower masses for binaries with antialigned spins.

Consistent with our expectation, we see in Fig. 6 (top left panel) that for a given mass ratio, at low masses, binaries with negative spins have higher ineffectualness but as the mass increases there is a crossover point beyond which binaries with positive spins have higher ineffectualness. While for positive spins, the ineffectualness continues to increase with total mass, for zero spins the ineffectualness plateaus and for negative spins it reaches a maximum value and starts decreasing beyond that point. We see from Fig. 6 that this trend of larger (smaller) effectualness for negative (positive) spins at high masses ( $M \gtrsim 100M_{\odot}$ ) is achieved at the cost of larger (smaller) systematic biases in the estimated parameters.

We set  $\text{FF}_{\text{eff}} \geq 0.965$  (which corresponds to a  $\sim 10\%$  loss in detection volume for a fixed SNR threshold) as the benchmark for the relative importance of nonquadrupole modes in detection. This is shown by the dashed black line in the top-left panel of Fig. 6. Figure 1a summarizes the region in the parameter space where the loss of detectable volume (at a fixed SNR threshold) due to neglecting nonquadrupole modes is greater than 10%. For the case of negative spins, even at large mass ratios, we see that subdominant modes are important for detection only over a range of masses ( $M \sim 75 - 150M_{\odot}$ ). For binaries with positive and zero spins, we anticipate that the upper limit of total mass where the higher modes are important

<sup>6</sup>Note that this is not true for the  $q \approx 1$  cases. For these, since the mismatches are quite small  $\sim 10^{-3}$ , several competing effects are playing out.



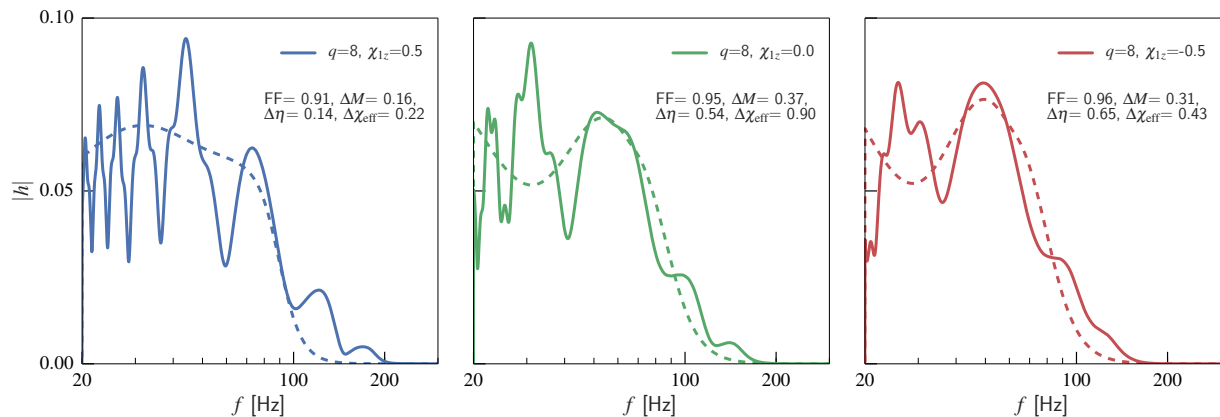


FIG. 7: Comparison of the frequency domain amplitudes of the “full” hybrid waveform containing subdominant modes (solid lines) and the best-match template waveforms containing only the quadrupole modes (dashed lines). The waveforms have been “whitened” according to the PSD used for match calculation and normalized such that the match with itself is unity. The orientation angles are chosen to be  $\iota = \pi/4$ ,  $\varphi_0 = \pi$ ,  $\psi = \pi/3$ . The total mass is  $M = 200 M_\odot$ , and the mass ratio is  $q = 8$ . The legends show the spin of the larger black hole. The spin on the smaller black hole is zero in all three cases. The inset text shows the fitting factor, fractional biases in parameters  $M$  and  $\eta$  and absolute bias in parameter  $\chi_{\text{eff}}$ , at the best-match point. Particularly in the case of negative spin, where the observed signal is dominated by the ringdown, we see that the template is able to mimic the target, producing a reasonably good fitting factor. But this comes at the expense of larger parameter biases.

is above  $300M_\odot$ , the highest mass that we consider in this study. Based on Fig. 1a, we expect the quadrupole mode templates to be fully effectual for detection either when  $q \lesssim 4$  or when  $M \lesssim 70M_\odot$  (irrespective of spins), considering a population of binaries distributed with isotropic orientations. We note that the region in which subdominant modes become important for detection is the smallest (largest) for negative (positive) spins.

Figure 1a also shows the region in the parameter space (marked by the green dashed line) where subdominant modes are important for the detection of nonspinning binaries when nonspinning quadrupole mode templates are used, obtained in our previous study [18]. We see that the use of quadrupole mode templates with nonprecessing spins has helped us to reduce the region in the parameter space where subdominant modes cause unacceptable loss in the detection volume. This is consistent with our expectation, as two additional parameters (spins) in the templates allow them to achieve higher fitting factors with the target signals, at the cost of a larger bias in the best-matched template parameters.

In order to gauge the relative importance of the systematic errors shown in Fig. 6, we compare them against the expected statistical errors from the quadrupole-mode template family IMR-PhenomD (computed using Fisher matrix formalism). Figure 8 shows the minimum SNR (orientation-averaged) at which the  $1\sigma$  statistical errors become low enough to equal the systematic errors. (Note that statistical errors are inversely proportional to the SNR.) We see that, at high masses, the systematic errors start to dominate the error budget for orientation-averaged SNRs as low as 3. In this study, whenever the systematic errors are less than the statistical error for an orientation-averaged SNR of 8 (horizontal black dashed line in Fig. 8), we regard the quadrupole-mode templates to be faithful for parameter estimation<sup>7</sup>.

<sup>7</sup>Note that, when full mode templates are employed in the parameter estimation, the statistical errors are expected to go down in general, due to the increased amount of information in the waveform (see, e.g., [63]). We do not consider this effect here.

Figure 1b summarizes the region in the parameter space where this minimum orientation-averaged SNR is less than or equal to 8 for estimation of any of  $M$ ,  $\eta$  or  $\chi_{\text{eff}}$ . We exclude any cases where the systematic biases are dominated by the biases in the quadrupole mode itself. We note that the region in which subdominant modes become important for parameter estimation is smallest (largest) for positive (negative) spins. This trend is opposite to what we see in Fig. 1a for detection. This is because, at high masses negative spin binaries have higher effectualness than positive spin binaries, which is achieved at the cost of higher systematic biases. We remind the reader that, for spins of higher magnitude than considered in this study (i.e.  $|\chi_{\text{eff}}| > 0.5$  for  $q \geq 2$ ), we expect the shaded regions in Fig. 1 to expand or reduce depending on the spin; the contours that we draw are indicative demarcations only. For greater aligned spins, the shaded region for detection should expand and the shaded region for parameter estimation should reduce. The opposite trend is expected for greater antialigned spins. Figure 1b also compares these results with the results obtained in our previous study [18] (dashed green line) using nonspinning quadrupole-only templates against nonspinning “full” target waveforms. We see that the use of spinning templates essentially increases the region where the parameter estimation bias is dominated by systematic errors.

#### IV. CONCLUSION

We studied the effects of sub-dominant modes in the detection and parameter estimation of GWs from black hole binaries with nonprecessing spins using Advanced LIGO detectors. The effect of sub-dominant modes on detection is quantified in terms of the effective detection volume (fraction of the optimal detection volume that the suboptimal search is sensitive to, for a given SNR threshold) and the effect on parameter estimation in terms of the effective bias (weighted average of the systematic errors for different orientations) in the estimated parameters. We compared quadrupole-mode templates with target signals (hybrid waveforms constructed by matching NR simulations



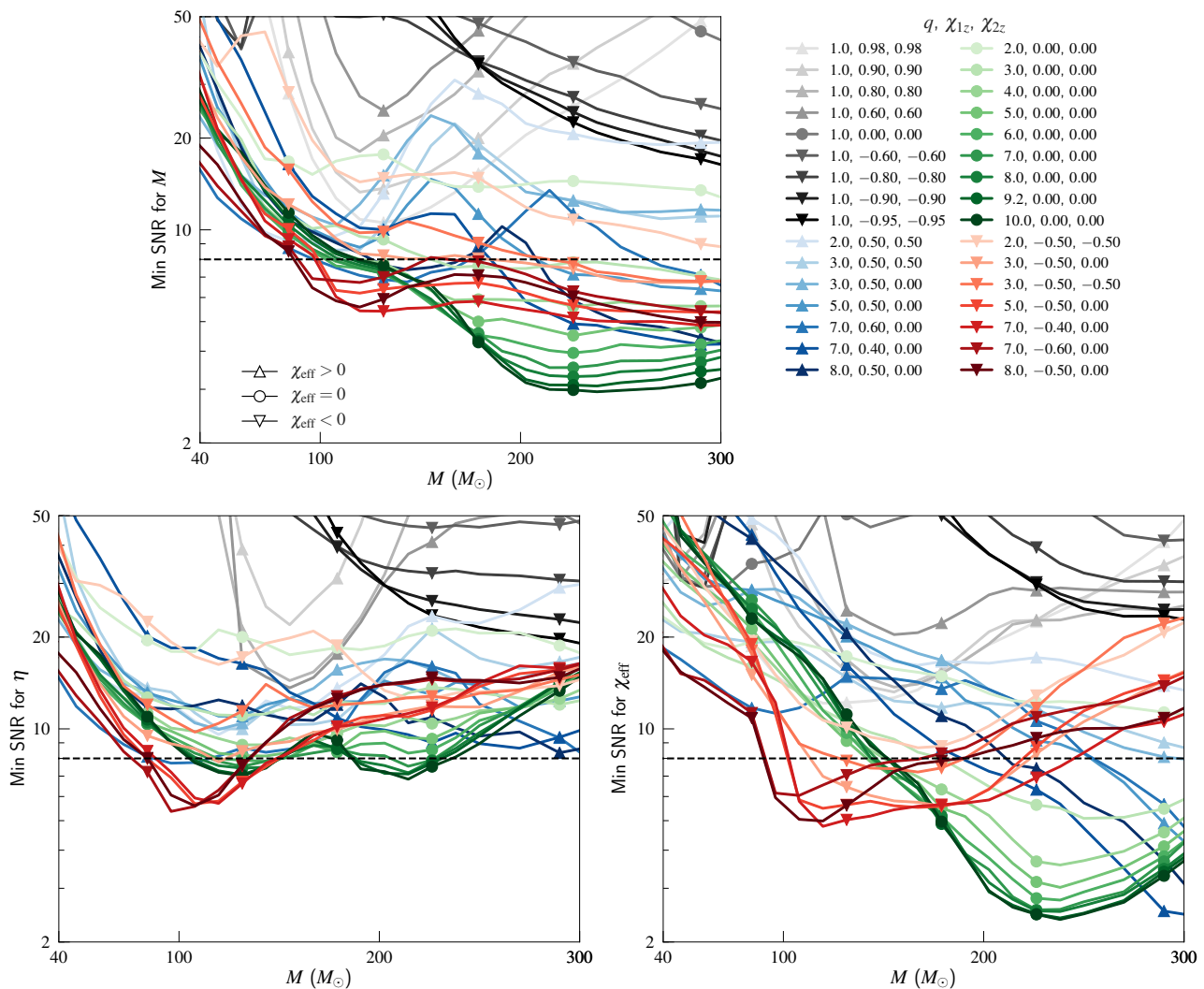


FIG. 8: Lowest SNR (orientation-averaged) at which the statistical errors are low enough to equal the effective systematic bias in parameters  $M$ ,  $\eta$ , and  $\chi_{\text{eff}}$ , when using quadrupole mode templates to estimate the parameters of hybrid waveforms including all modes. A dashed black line is used to denote minimum orientation-averaged SNR of 8 (optimal orientation SNR of 20).

describing the late inspiral, merger and ringdown with PN/EOB waveforms describing the early inspiral). These signals contained contributions from all the spherical harmonic modes up to  $\ell = 4$  and  $-\ell \leq m \leq \ell$  except the  $m = 0$  modes.

Our study considered black hole binaries with total masses  $40M_{\odot} \leq M \leq 300M_{\odot}$ , mass ratios  $1 \leq q \leq 10$ , and various spins including  $\chi_{\text{eff}} \sim -0.5, 0, 0.5$  ( $|\chi_{\text{eff}}| \leq 0.98$  for  $q = 1$ ). The results are appropriately averaged over all angles describing the orientation of the binary (the results are not explicitly averaged over the sky location because both the fitting factors and systematic biases are only weakly dependent on the sky location<sup>3</sup>). Figure 1 shows the regions in the parameter space where the contribution from nonquadrupole modes is important for GW detection and parameter estimation. In general, neglecting subdominant modes can cause unacceptable loss of SNR and unacceptably large systematic errors for binaries with high masses and large mass ratios. For a given mass ratio, subdominant modes are more important for positive (negative) spins for detection (parameter estimation). As compared to our previous study restricted to the case of nonspinning binaries, we see that the use of quadrupole mode templates with nonprecessing spins, enhances the effectualness for detection, but extends the region where systematic errors dominate.

Note that the scope of our study was rather restricted – while

we conclude that subdominant mode templates are likely to improve the detection rates of binary black holes in certain regions in the parameter space (high mass and large mass ratios), a proper characterization of this will require characterizing the associated increase in the false alarm rate also (see, e.g., Ref. [22]). Also, we did not study the effect of neglecting nonquadrupole modes on signal-based vetoes such as the “chi-square” veto [64]. Similarly, we have only investigated the region in the parameter space where the use of the quadrupole-only template would introduce systematic errors that are larger than the expected statistical errors. However, the use of full-mode templates in parameter estimation is likely to reduce the statistical errors, owing to the increased information content in the waveform. We have not explored this aspect of the problem here. The expected statistical errors were estimated using the Fisher matrix formalism. Since these error bounds are lower limits, our estimates on the region of the parameter space where the systematic errors are negligible should be treated as conservative estimates. We conclude that subdominant modes are important for parameter estimation when the systematic errors are greater than  $1\sigma$  statistical errors at a sky and orientation averaged SNR of 8. If more stringent criteria are applied, our shaded regions in Fig. 1b would widen. Also, note that we restricted our study to the case of binaries with nonprecessing

spins. Astrophysical black hole binaries may have generic spin orientations. It is not clear how our conclusions hold in the case of precessing spins (see Ref. [65] for some recent work in this direction). We leave some of these investigations as future work.

### Appendix A: Comparison with Bayesian parameter estimation

In this paper, we tried to quantify the loss of detection efficiency due to neglecting subdominant modes by computing the fitting factors of the dominant-mode templates with target signals including the effect of subdominant modes. Systematic errors in parameter estimation were computed by comparing the parameters of the “best-matched” subdominant-mode templates with the true parameters of the target signals, while statistical errors are computed from the Fisher information matrix. Since these calculations are computationally inexpensive, this allows us to study the impact of subdominant modes over the entire parameter space of interest, after averaging over extrinsic parameters such as the orientation angles. However, we know that the inverse of the Fisher matrix provides a *lower bound* of the statistical errors in the parameter estimation [66, 67]. In order to verify that our simplified estimates of the statistical and systematic errors give a good approximation to the true errors, we compare our estimates of the systematic and statistical errors with those derived from full Bayesian parameter estimation for one sample case.

We create a simulated data stream by injecting a numerical-relativity waveform from the SXS waveform catalog [31, 33, 68] into colored Gaussian noise with the power spectrum of Advanced LIGO. The injected waveform (SXS:BBH:0307) has the mass ratio  $m_1/m_2 = 1.228$ , aligned spins  $\chi_1 = 0.32$ ,  $\chi_2 = -0.5798$ , and has a SNR of  $\sim 25$ . We estimate the posterior distributions of the masses and spins using the LALINFERENCE\_NEST code [16, 69] that is part of the LSC Algorithms Library [70]. We compare the maximum a posteriori probability (MAP) estimates with the true parameters, which

provides us an estimate of the systematic bias. Similarly, the width of the 68% credible regions provides us an estimate of the statistical errors. These estimates are compared with the same estimated using the methods that we use in the paper. Table II provides a comparison between these independent estimates. We see that, for the parameters that we consider, the two different estimates are in reasonable agreement. Although this provides some confidence in our results, extensive comparisons with Bayesian estimates over the full parameters space are required to confidently establish the accuracy of our approximate results. We leave this as future work.

### Acknowledgments

We are indebted to the SXS Collaboration for making a public catalog of numerical-relativity waveforms, and to Chandra Kant Mishra for sharing a notebook of post-Newtonian waveforms. We thank Abhirup Ghosh, Chandra Kant Mishra, Sascha Husa, Mark Hannam, Michael Pürrer, and Patricia Schmidt for useful discussions. We also thank Richard O’Shaughnessy, B. S. Sathyaprakash, Prayush Kumar, and the anonymous referee for several useful comments on the manuscript. P. A.’s research was supported by the AIRBUS Group Corporate Foundation through a chair in “Mathematics of Complex Systems” at the International Centre for Theoretical Sciences (ICTS); by a Ramanujan Fellowship from the Science and Engineering Research Board (SERB), India; by the SERB FastTrack fellowship SR/FTP/PS-191/2012; by Indo-US Centre for the Exploration of Extreme Gravity funded by the Indo-US Science and Technology Forum; and by the Max Planck Society and the Department of Science and Technology, India, through a Max Planck Partner Group at ICTS. V. V.’s research was supported by NSF Grant No. PHY-1404569 to Caltech and the Sherman Fairchild Foundation. Computations were performed at the ICTS clusters Mowgli, Dogmatix, and Alice.

- 
- [1] B. P. Abbott et al. (LIGO Scientific Collaboration and Virgo Collaboration), Phys. Rev. Lett. **116**, 061102 (2016), URL <http://link.aps.org/doi/10.1103/PhysRevLett.116.061102>.
  - [2] B. P. Abbott et al. (LIGO Scientific Collaboration and Virgo Collaboration), Phys. Rev. Lett. **116**, 241103 (2016), URL <http://link.aps.org/doi/10.1103/PhysRevLett.116.241103>.
  - [3] B. P. Abbott et al. (LIGO Scientific Collaboration), ArXiv e-prints (2016), 1602.03842.
  - [4] B. P. Abbott et al. (LIGO Scientific Collaboration and Virgo Collaboration), Phys. Rev. X **6**, 041015 (2016), URL <http://link.aps.org/doi/10.1103/PhysRevX.6.041015>.
  - [5] B. P. Abbott et al. (LIGO Scientific Collaboration and Virgo Collaboration), Phys. Rev. Lett. **116**, 241102 (2016), URL <http://link.aps.org/doi/10.1103/PhysRevLett.116.241102>.
  - [6] B. P. Abbott et al. (LIGO Scientific Collaboration), The Astrophysical Journal Letters **818**, L22 (2016), 1602.03846.
  - [7] B. P. Abbott et al. (LIGO Scientific and Virgo Collaborations), Phys. Rev. Lett. **116**, 221101 (2016), URL <http://link.aps.org/doi/10.1103/PhysRevLett.116.221101>.
  - [8] S. Klimentenko et al., Phys. Rev. **D93**, 042004 (2016), 1511.05999.
  - [9] R. Lynch, S. Vitale, R. Essick, E. Katsavounidis, and F. Robinet (2015), 1511.05955.
  - [10] S. Klimentenko, I. Yakushin, A. Mercer, and G. Mitselmakher, Classical and Quantum Gravity **25**, 114029 (2008), URL <http://stacks.iop.org/0264-9381/25/i=11/a=114029>.
  - [11] B. P. Abbott et al. (LIGO Scientific Collaboration and Virgo Collaboration), Phys. Rev. D **93**, 122004 (2016), URL <http://link.aps.org/doi/10.1103/PhysRevD.93.122004>.
  - [12] B. P. Abbott et al. (LIGO Scientific Collaboration and Virgo Collaboration), Phys. Rev. D **93**, 122003 (2016), URL <http://link.aps.org/doi/10.1103/PhysRevD.93.122003>.
  - [13] T. Dal Canton et al., Phys. Rev. **D90**, 082004 (2014), 1405.6731.
  - [14] S. A. Usman et al., Class. Quant. Grav. **33**, 215004 (2016), 1508.02357.
  - [15] K. Cannon et al., Astrophys. J. **748**, 136 (2012), 1107.2665.
  - [16] J. Veitch et al., Phys. Rev. **D91**, 042003 (2015), 1409.7215.
  - [17] T. Damour, B. R. Iyer, and B. S. Sathyaprakash, Phys. Rev. D **57**, 885 (1998).
  - [18] V. Varma, P. Ajith, S. Husa, J. C. Bustillo, M. Hannam, and M. Pürrer, Phys. Rev. D **90**, 124004 (2014), URL <http://link.aps.org/doi/10.1103/PhysRevD.90.124004>.
  - [19] B. P. Abbott et al. (Virgo, LIGO Scientific), Phys. Rev. D **94**, 064035 (2016), 1606.01262.
  - [20] L. Pekowsky, J. Healy, D. Shoemaker, and P. Laguna, Phys. Rev. D **87**, 084008 (2013).
  - [21] D. A. Brown, P. Kumar, and A. H. Nitz, Phys. Rev. D **87**, 082004 (2013).
  - [22] C. Capano, Y. Pan, and A. Buonanno (2013), 1311.1286.
  - [23] B. P. Abbott et al. (the Virgo, The LIGO Scientific) (2016), 1611.07531.

Method	$M_{\text{bias}}$	$\eta_{\text{bias}}$	$\chi_{\text{bias}}^{\text{eff}}$	$\delta M$	$\delta \eta$	$\delta \chi_{\text{eff}}$
Bayesian	$7.6 \times 10^{-1} M_{\odot}$	$2.2 \times 10^{-3}$	$4.3 \times 10^{-2}$	$2.8 M_{\odot}$	$2.4 \times 10^{-3}$	$1.3 \times 10^{-1}$
FF/Fisher	$2.6 \times 10^{-1} M_{\odot}$	$2.7 \times 10^{-3}$	$5.4 \times 10^{-2}$	$1.9 M_{\odot}$	$9.5 \times 10^{-3}$	$7.0 \times 10^{-2}$

TABLE II: Comparison of systematic and statistical biases as predicted by a full Bayesian parameter estimation (top row) study with a fitting factor/Fisher matrix study that is used in this paper (bottom row). The first three columns show the absolute systematic biases and the next three columns show the statistical errors in the estimation of total mass  $M$ , symmetric mass ratio  $\eta$  and effective spin  $\chi_{\text{eff}}$ . For the Bayesian study (top row), systematic biases are inferred from the peaks of the posterior distributions and the statistical biases are given by the widths of 68% credible intervals. In the bottom row, the systematic biases are inferred from the best-match parameters and the statistical biases are given by  $1\sigma$  errors from a Fisher matrix study.

- [24] B. P. Abbott et al. (LIGO Scientific Collaboration and Virgo Collaboration), Phys. Rev. D **94**, 064035 (2016), URL <http://link.aps.org/doi/10.1103/PhysRevD.94.064035>.
- [25] J. Calderón Bustillo, S. Husa, A. M. Sintes, and M. Pürrer, Phys. Rev. D **93**, 084019 (2016), URL <http://link.aps.org/doi/10.1103/PhysRevD.93.084019>.
- [26] B. Sathyaprakash and B. F. Schutz, Living Reviews in Relativity **12** (2009), URL <http://www.livingreviews.org/lrr-2009-2>.
- [27] L. Blanchet, G. Faye, B. R. Iyer, and S. Sinha, Class.Quant.Grav. **25**, 165003 (2008), 0802.1249.
- [28] K. G. Arun, A. Buonanno, G. Faye, and E. Ochsner, Phys. Rev. D **79**, 104023 (2009), URL <http://link.aps.org/doi/10.1103/PhysRevD.79.104023>.
- [29] A. Buonanno, G. Faye, and T. Hinderer, Phys. Rev. **D87**, 044009 (2013), 1209.6349.
- [30] A. Taracchini, A. Buonanno, Y. Pan, T. Hinderer, M. Boyle, D. A. Hemberger, L. E. Kidder, G. Lovelace, A. H. Mroué, H. P. Pfeiffer, et al., Phys. Rev. D **89**, 061502 (2014), URL <http://link.aps.org/doi/10.1103/PhysRevD.89.061502>.
- [31] SXS Gravitational Waveform Database, URL <http://www.black-holes.org/waveforms/>.
- [32] The Spectral Einstein Code, URL <http://www.black-holes.org/SpEC.html>.
- [33] A. H. Mroue, M. A. Scheel, B. Szilagyi, H. P. Pfeiffer, M. Boyle, et al. (2013), 1304.6077.
- [34] A. H. Mroue and H. P. Pfeiffer (2012), 1210.2958.
- [35] G. Lovelace, M. Scheel, and B. Szilagyi, Phys.Rev. **D83**, 024010 (2011), 1010.2777.
- [36] J. Blackman, S. E. Field, C. R. Galley, B. Szilagyi, M. A. Scheel, M. Tiglio, and D. A. Hemberger, Phys. Rev. Lett. **115**, 121102 (2015), 1502.07758.
- [37] L. T. Buchman, H. P. Pfeiffer, M. A. Scheel, and B. Szilagyi, Phys.Rev. **D86**, 084033 (2012), 1206.3015.
- [38] S. Ossokine, L. E. Kidder, and H. P. Pfeiffer, Phys.Rev. **D88**, 084031 (2013), 1304.3067.
- [39] D. A. Hemberger, M. A. Scheel, L. E. Kidder, B. Szilagyi, G. Lovelace, et al., Class.Quant.Grav. **30**, 115001 (2013), 1211.6079.
- [40] B. Szilagyi, L. Lindblom, and M. A. Scheel, Phys.Rev. **D80**, 124010 (2009), 0909.3557.
- [41] M. Boyle and A. H. Mroue, Phys.Rev. **D80**, 124045 (2009), 0905.3177.
- [42] M. A. Scheel, M. Boyle, T. Chu, L. E. Kidder, K. D. Matthews, et al., Phys.Rev. **D79**, 024003 (2009), 0810.1767.
- [43] M. Boyle et al., Phys. Rev. **D76**, 124038 (2007), 0710.0158.
- [44] M. A. Scheel, H. P. Pfeiffer, L. Lindblom, L. E. Kidder, O. Rinne, et al., Phys.Rev. **D74**, 104006 (2006), gr-qc/0607056.
- [45] L. Lindblom, M. A. Scheel, L. E. Kidder, R. Owen, and O. Rinne, Class.Quant.Grav. **23**, S447 (2006), gr-qc/0512093.
- [46] H. P. Pfeiffer, L. E. Kidder, M. A. Scheel, and S. A. Teukolsky, Comput.Phys.Commun. **152**, 253 (2003), gr-qc/0202096.
- [47] D. A. Hemberger, G. Lovelace, T. J. Loredo, L. E. Kidder, M. A. Scheel, et al., Phys.Rev. **D88**, 064014 (2013), 1305.5991.
- [48] I. MacDonald, A. H. Mroue, H. P. Pfeiffer, M. Boyle, L. E. Kidder, M. A. Scheel, B. Szilagyi, and N. W. Taylor, Phys. Rev. **D87**, 024009 (2013), 1210.3007.
- [49] I. MacDonald, S. Nissanke, H. P. Pfeiffer, and H. P. Pfeiffer, Class. Quant. Grav. **28**, 134002 (2011), 1102.5128.
- [50] M. Hannam, S. Husa, U. Sperhake, B. Bruegmann, and J. A. Gonzalez, Phys. Rev. **D77**, 044020 (2008), 0706.1305.
- [51] P. Ajith, Class. Quant. Grav. **25**, 114033 (2008).
- [52] M. Hannam, S. Husa, F. Ohme, and P. Ajith, Phys. Rev. **D82**, 124052 (2010), 1008.2961.
- [53] S. Khan, S. Husa, M. Hannam, F. Ohme, M. Pürrer, X. J. Forteza, and A. Bohé, Phys. Rev. D **93**, 044007 (2016), URL <http://link.aps.org/doi/10.1103/PhysRevD.93.044007>.
- [54] S. Husa, S. Khan, M. Hannam, M. Pürrer, F. Ohme, X. J. Forteza, and A. Bohé, Phys. Rev. D **93**, 044006 (2016), URL <http://link.aps.org/doi/10.1103/PhysRevD.93.044006>.
- [55] LALSimulation is part of the LALSuite software package, URL <https://www.lsc-group.phys.uwm.edu/daswg/projects/lalsuite.html>.
- [56] T. A. Apostolatos, Phys. Rev. D **52**, 605 (1995).
- [57] B. Allen, W. G. Anderson, P. R. Brady, D. A. Brown, and J. D. E. Creighton, Phys. Rev. **D85**, 122006 (2012), gr-qc/0509116.
- [58] The SciPy software library, URL <http://scipy.org/>.
- [59] *Advanced LIGO anticipated sensitivity curves*, LIGO Document T0900288-v3, URL <https://dcc.ligo.org/LIGO-T0900288/public>.
- [60] S. Vitale, Phys. Rev. **D94**, 121501 (2016), 1610.06914.
- [61] M. Campanelli, C. O. Lousto, and Y. Zlochower, Phys. Rev. D **74**, 041501 (2006), URL <http://link.aps.org/doi/10.1103/PhysRevD.74.041501>.
- [62] M. Hannam, S. Husa, B. Brügmann, and A. Gopakumar, Phys. Rev. D **78**, 104007 (2008), URL <http://link.aps.org/doi/10.1103/PhysRevD.78.104007>.
- [63] C. Van Den Broeck and A. S. Sengupta, Class.Quant.Grav. **24**, 155 (2007), gr-qc/0607092.
- [64] B. Allen, Phys. Rev. **D71**, 062001 (2005), gr-qc/0405045.
- [65] J. C. Bustillo, P. Laguna, and D. Shoemaker, p. 6 (2016), 1612.02340, URL <http://arxiv.org/abs/1612.02340>.
- [66] H. Cramér, *Mathematical Methods of Statistics*, Princeton Mathematical Series (Princeton University Press, 1999), ISBN 9780691005478, URL <https://books.google.co.in/books?id=CRTKKaJ00DYC>.
- [67] C. Radhakrishna Rao, Bull. Calcutta Math. Soc. **37**, 81 (1945), ISSN 0008-0659.
- [68] P. Schmidt, I. W. Harry, and H. P. Pfeiffer (2017), 1703.01076.
- [69] J. Veitch and A. Vecchio, Phys. Rev. D **81** (2010), 0911.3820.
- [70] *LSC Algorithms Library*, URL <https://www.lsc-group.phys.uwm.edu/daswg/projects/lalsuite.html>.